


The Effect of Anchor Group on the Phonon Thermal Conductance of Single Molecule Junctions

Mohammed D. Noori^{1,2}, Sara Sangtarash¹ and Hatéf Sadeghi^{1,*} 

¹ Device Modelling Group, School of Engineering, University of Warwick, Coventry CV4 7AL, UK; mdn.noori@sci.utq.edu.iq (M.D.N.); Sara.Sangtarash@warwick.ac.uk (S.S.)

² Department of Physics, College of Sciences, University of Thi-Qar, Thi-Qar 64001, Iraq

* Correspondence: Hatéf.Sadeghi@warwick.ac.uk

Abstract: There is a worldwide race to convert waste heat to useful energy using thermoelectric materials. Molecules are attractive candidates for thermoelectricity because they can be synthesised with the atomic precision, and intriguing properties due to quantum effects such as quantum interference can be induced at room temperature. Molecules are also expected to show a low thermal conductance that is needed to enhance the performance of thermoelectric materials. Recently, the technological challenge of measuring the thermal conductance of single molecules was overcome. Therefore, it is timely to develop strategies to reduce their thermal conductance for high performance thermoelectricity. In this paper and for the first time, we exploit systematically the effect of anchor groups on the phonon thermal conductance of oligo (phenylene ethynylene) (OPE3) molecules connected to gold electrodes via pyridyl, thiol, methyl sulphide and carbodithioate anchor groups. We show that thermal conductance is affected significantly by the choice of anchor group. The lowest and highest thermal conductances were obtained in the OPE3 with methyl sulphide and carbodithioate anchor groups, respectively. The thermal conductance of OPE3 with thiol anchor was higher than that with methyl sulphide but lower than the OPE3 with pyridyl anchor group.



Citation: Noori, M.D.; Sangtarash, S.; Sadeghi, H. The Effect of Anchor Group on the Phonon Thermal Conductance of Single Molecule Junctions. *Appl. Sci.* **2021**, *11*, 1066. <https://doi.org/10.3390/app11031066>

Academic Editor: Linda Angela Zotti
Received: 26 December 2020
Accepted: 21 January 2021
Published: 25 January 2021

Publisher's Note: MDPI stays neutral with regard to jurisdictional claims in published maps and institutional affiliations.



Copyright: © 2021 by the authors. Licensee MDPI, Basel, Switzerland. This article is an open access article distributed under the terms and conditions of the Creative Commons Attribution (CC BY) license (<https://creativecommons.org/licenses/by/4.0/>).

Keywords: molecular electronics; thermoelectricity; phonon; thermal conductance; OPE3; anchor groups; pyridyl; thiol; methyl sulphide; carbodithioate

1. Introduction

Currently, nearly 10% of the world's electricity is used by computers and the internet and converted to heat. This waste heat could be used to generate electricity economically, provided materials with a high thermoelectric efficiency could be identified [1]. The demand for new thermoelectric materials has led to a worldwide race to develop materials with a high thermoelectric efficiency [2–11]. The efficiency of a thermoelectric device is inversely proportional to its thermal conductance $\kappa = \kappa_p + \kappa_e$ due to electrons (κ_e) and phonons (κ_p) [12]. Therefore, low-thermal-conductance materials are needed for an efficient conversion of heat into electricity. The state of the art thermoelectric figure of merit (ZT) was found in inorganic materials, e.g., 2.2 at high temperatures 900 K [13]. These inorganic materials are toxic, and their global supply is limited. Therefore, organic materials are now being considered [14].

Molecules are attractive candidates for thermoelectricity because their structure can be modified with atomic precision and desirable properties can be induced by the engineering of their structure [15,16]. They are also expected to show intriguing properties, such as room temperature quantum and phonon interference, that can be used to simultaneously increase their electrical conductance and Seebeck coefficient and to suppress their thermal conductance [17,18].

Just recently the technological challenge of measuring the thermal conductance of single molecules was overcome [19,20]. This opens new avenues to study the thermoelectric efficiency of single molecules [21,22]. To optimize molecular junctions for a maximum

efficiency, strategies to increase their electrical conductance and Seebeck coefficient simultaneously and to suppress their thermal conductance should be developed. So far, thermal conductance of a few molecules, including C60 [23], alkanes [19,24], OPE2 derivatives [17], OPE3 [19,23], Benzene [25,26], Oligoynes [24], biphenyl-dithiol [17], bipyridyl and its radical counterpart [18], between gold electrodes has been calculated. Among these, thermal conductance of alkanes [19,20] and OPE3 [27] molecules with thiol anchor were measured. Table 1 shows a summary of room temperature thermal conductance calculations due to electrons (κ_e) and phonons (κ_p) of single molecules between gold electrodes using density functional theory (DFT) combined with the non-equilibrium Green's function (NEGF) method for transport calculations and comparison with single molecule thermal conductance measurements. Previous studies show that the thermal conductance of single molecules is dominated by phonons. For example, the measured thermal conductance of OPE3 is 20 ± 6 pW/K [27]. The calculated contribution from electrons and phonons are 0.1 pW/K and 19 pW/K, respectively [27]. The thermal conductance can be controlled using electrically inert side groups and phonon interference through multipath molecular backbones [17,25,26,28,29].

Table 1. Room temperature thermal conductance due to electrons (κ_e) and phonons (κ_p) of single molecules between gold electrodes using DFT-NEGF calculations and single molecule measurements.

Molecule	Calculated κ (pW/K)		Measured κ (pW/K)	Ref.	
	κ_p	κ_e at DFT Fermi Energy			
Biphenyl-4,4'-dithiol (BDT)	19.6	2.3	-	[17]	
2,2'-dinitro-BDT	11.7	<0.01	-	[17]	
oligo(2-phenylene-4,4'-ethynylene)-dithiol (OPE2)	9.9	<0.01	-	[17]	
2,2'-dinitro-OPE2	9.7	16.7	-	[17]	
4,4'-bipyridyl (BP)	34.8	<0.01	-	[17]	
3,3',5,5'-tetrachloride-BP	14.8	<0.01	-	[17]	
3,3'-dinitro-BP	23.6	<0.01	-	[17]	
oligo(3-phenylene-4,4'-ethynylene)-dithiol (OPE3)	19	0.1	20 ± 6	[19]	
Octane-dithiol	23	0.02	29 ± 8	[19]	
Alkanes with dihydrobenzo[b]thiophene (BT) anchor ($N =$ number of C_2H_4)	$N = 1$	25.4	0.03	-	[24]
	$N = 2$	33.4	<0.01	-	[24]
	$N = 4$	30.3	<0.01	-	[24]
	$N = 8$	5.6	<0.01	-	[24]
Alkanedithiol ($N =$ number of C_2H_4)	$N = 1$	17–22	5.7	14.6 ± 3	[20]
	$N = 2$	18–27	1.1	13.4 ± 5	[20]
	$N = 3$	17–29	<0.01	16.9 ± 3	[20]
	$N = 4$	20–33	<0.01	26.3 ± 7	[20]
	$N = 5$	17–33	<0.01	28 ± 8	[20]
Oligoynes with BT anchor ($N =$ number of C_2H_4)	$N = 1$	15.6	0.4	-	[24]
	$N = 2$	9.2	0.5	-	[24]
	$N = 4$	7.7	0.25	-	[24]

Table 1. Cont.

Molecule	Calculated κ (pW/K)		Measured κ (pW/K)	Ref.
	κ_p	κ_e at DFT Fermi Energy		
2,2'-bipyridine-BP	6	0.3	-	[18]
BP functionalized with tert-butyl nitroxide radical	2	1.45	-	[18]
C ₆₀ monomer	20–46.3	68–572	-	[23]
C ₆₀ dimer	7–7.3	0.1–1.8	-	[23]
Benzenedithiol	meta	7.5	-	[26]
	para	22.5	-	
Benzenediamine	meta	24.5	-	[25]
	para	25.2	-	
2-fluoro-1,4-diaminobenzene	24.4	2.62	-	[25]
2-chloro-1,4-diaminobenzene	22.2	2.7	-	[25]
2-bromo-1,4-diaminobenzene	16.9	2.8	-	[25]
2,5-dibromo-1,4-diaminobenzene	17.9	2.9	-	[25]
2,6-dibromo-1,4-diaminobenzene	10.5	2.9	-	[25]
2,3-dibromo-1,4-diaminobenzene	18	3	-	[25]
OPE3-diamine	meta	13.8	0.11	[25]
	para	24.5	<0.01	[25]

In most of the molecular junctions, molecules are contacted to the electrodes via suitable anchor groups [30]. From Table 1, the calculated thermal conductance of alkanes is different in [24] (Alkanes with dihydrobenzo[b]thiophene (BT) anchor) and [20] (Alkanedithiol). While the electrodes and the molecular backbone are the same, these calculations use different anchor groups for alkanes. Therefore, it seems that the anchor group plays a significant role in the thermal conductance of molecules. In order to understand the effect of anchor groups on thermal conductance, a systematic study of a given molecular backbone with different anchor groups is needed. For this reason, we choose OPE3 and exploited its thermal conductance with different anchor groups including pyridyl (PY), thiol (S), methyl sulphide (SMe) and carbodithioate (CS) between two gold electrodes (see Figure 1). We found that thermal conductance due to phonons is affected significantly by the choice of anchor groups. For example, thermal conductance of OPE3 decreased by a factor of 2 from CS to SMe. This is significant because the thermoelectric figure of merit (ZT) is inversely proportional to thermal conductance, and therefore ZT can be enhanced by a factor of 2 using the choice of a suitable anchor group.

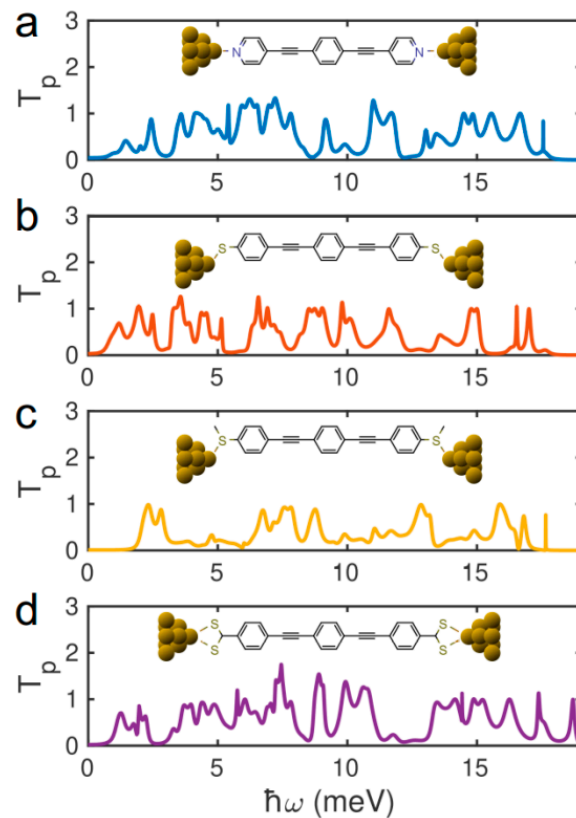


Figure 1. Phonon transmission coefficient versus phonons with energy $\hbar\omega$ for OPE3 with different anchor groups: (a) pyridyl PY, (b) thiol S, (c) methyl sulphide SMe and (d) carbodithioate CS.

2. Results and Discussion

To study vibrational and thermal properties of junctions formed by OPE3 and different anchor groups, the geometry of OPE3 in gas phase and between gold electrodes was relaxed to the force tolerance of $5 \text{ meV}/\text{\AA}$ using the SIESTA [31] implementation of density functional theory (DFT), with a double- ζ polarized basis set (DZP) and the local density approximation (LDA) functional with Ceperley and Alder (CA) parameterization. A real-space grid was defined with an equivalent energy cut-off of 350 Ry. Following the method described in [12,24], a set of xyz coordinates were generated by displacing each atom from the relaxed xyz geometry in the positive and negative x, y and z directions with $\delta q_l = 0.01 \text{ \AA}$. The forces $F_i^q = (F_i^x, F_i^y, F_i^z)$ in three directions $q_i = (x_i, y_i, z_i)$ on each atom were then calculated and used to construct the dynamical matrix $D_{ij} = K_{ij}^{qq'}/M_{ij}$ where the mass matrix $M = \sqrt{M_i M_j}$ and $K_{ij}^{qq'} = [F_i^q(\delta q_j^{q'}) - F_j^q(-\delta q_i^q)]/2\delta q_j^q$ for $i \neq j$ obtained from finite differences. To satisfy momentum conservation, the K for $i = j$ (diagonal terms) was calculated from $K_{ii} = -\sum_{i \neq j} K_{ij}$.

The phonon transmission $T_p(\omega)$ can then be calculated from the relation $T_p(\omega) = \text{Trace}(\Gamma_L^p(\omega) G_p^R(\omega) \Gamma_R^p(\omega) G_p^{R\dagger}(\omega))$ where $\Gamma_{L,R}^p(\omega) = i(\sum_{L,R}^p(\omega) - \sum_{L,R}^{p\dagger}(\omega))$ describes the level broadening due to the coupling to the left (L) and right (R) electrodes, $\sum_{L,R}^p(\omega)$ is the retarded self-frequencies associated with this coupling and $G_p^R = (\omega^2 I - D - \sum_L^p - \sum_R^p)^{-1}$ is the retarded Green's function, where D and I are the dynamical and the unit matrices, respectively.

Figure 1 shows the phonon transmission coefficient T_p for phonons with energy $\hbar\omega$ traversing from one gold electrode to the other through OPE3 derivatives with different anchor groups. T_p was limited to phonons with energies $\hbar\omega < 19 \text{ meV}$, which is the Debye frequency of Au electrodes [24]. The amplitude of T_p was generally higher for OPE3 with

the pyridyl PY (Figure 1a) and carbodithioate CS (Figure 1d) anchors. The amplitude of T_p was noticeably lower for OPE3 with the methyl sulphide SMe anchor (Figure 1c) compared to that with the thiol S anchor (Figure 1b). This is due to a combination of two effects. First, our calculations show that the binding energy between Au-S in SMe (0.47 eV) was weaker than that of Au-S in thiol (2.08 eV). This is because SMe makes a coordination bond to Au whereas the bond between Au-S in thiol is a stronger covalent bond. This means that the vibrational coupling between Au-S is stronger with thiol compared to the SMe anchor. Secondly, phonon interference [17] due to CH₃ side group in SMe led to the suppression of T_p . The phonon waves transmitted through sulphur atoms interfered destructively with the reflected waves by CH₃ groups for given frequencies, leading to the suppression of T_p . This is like a guitar string, where waves with certain frequencies are suppressed by pressing the string at different points.

Using T_p , the phonon thermal conductance κ_p at temperature T was calculated from $\kappa_p(T) = (2\pi)^{-1} \int_0^\infty \hbar\omega T_p(\omega) (\partial f_{BE}(\omega, T) / \partial T) d\omega$ where $f_{BE}(\omega, T) = (e^{\hbar\omega/k_B T} - 1)^{-1}$ is the Bose-Einstein distribution function, \hbar is the reduced Planck's constant and k_B is the Boltzmann's constant [12]. Figure 2 shows thermal conductance for OPE3 with the PY, S, SMe and CS anchor groups. κ_p increases with temperature T and saturates for temperatures higher than 150 K. This saturation of κ_p is mainly because of the small Debye frequency of gold electrodes [24]. The order of thermal conductances for different anchors is as follows: OPE3-CS (34 pW/K) > OPE3-PY (30 pW/K) > OPE3-S (25 pW/K) > OPE3-SMe (19 pW/K). Clearly, thermal conductance due to phonons is influenced strongly by the choice of anchor groups and the lowest thermal conductance is obtained for the molecule with the SMe anchor group. The thermal conductance of OPE3 with the SMe anchor was about two times lower than that with the CS anchor.

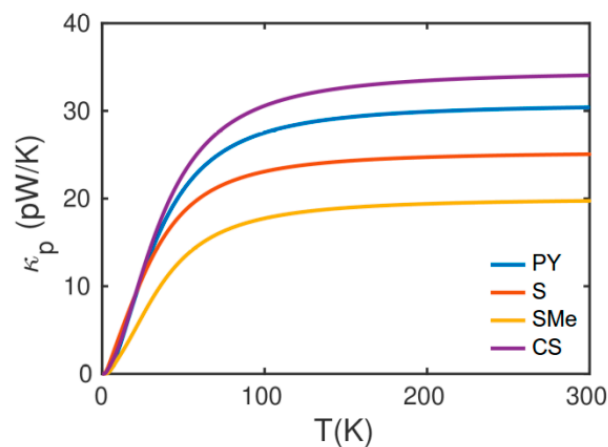


Figure 2. Phonon thermal conductance versus temperature T for OPE3 with different anchor groups.

To understand the DFT result further, we construct a simple tight binding (TB) model of ball and springs with one degree of freedom per site and the spring constant $\gamma = 61.3 \times 10^{-3} eV$ (Figure 3a) connected to two one dimensional leads through a weak coupling. Figure 3b shows the phonon transmission coefficient using the TB model for junctions with different anchor groups. Note that for simplicity, we have considered all spring constants γ the same. The phonon thermal conductance showed a similar trend to the DFT result $\kappa_p^{CS} > \kappa_p^{PY} > \kappa_p^S > \kappa_p^{SMe}$. The only difference between the junction with S and SMe anchors is the additional pendent side groups in SMe (Figure 3a). These pendent side groups attached to S clearly leads to the suppression of T_p resonances for the high frequency phonons and consequently to the decrease of the thermal conductance in OPE3 with the SMe anchor groups. The width of the T_p resonances with the CS anchor group was larger. CS anchors were connected to the electrodes from two points (inset of Figure 1d); thus the overall coupling strength to electrodes is higher. This leads to the larger broadening of T_p resonances in OPE3 with the CS anchor groups, leading to a high

thermal conductance. Note that thermal conductance is proportional to the area under T_p curve that increases when width of a resonance increases.

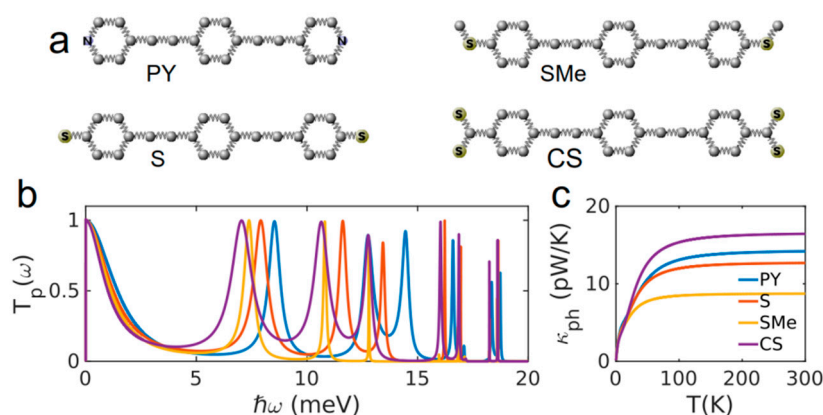


Figure 3. Tight binding (TB) model. (a) A simple ball and spring TB model with one degree of freedom per atom connected to two one dimensional leads through the weak coupling, (b) phonon transmission coefficient T_p for phonons with frequencies ω and (c) phonon thermal conductance versus temperature T for the simple TB model in (a).

The thermal conductance of OPE3 with the PY anchor is larger than that of with the S anchor. The only difference between these two junctions in the simple TB model is the additional sites at the two ends of the molecule (Figure 3a). There are two competing effects associated with this. First, the level spacing between resonances decreases when the size of the system (the number of atoms) increases. As a result, the thermal conductance is expected to increase because more resonances moved into the energy window defined by the Bose–Einstein distribution function at room temperature. Secondly, the resonance width decreases. This is because the length of the junction increases and, consequently, the density of phonon state at the two end points decreases, leading to the smaller broadening of the resonances. Clearly, the first effect is dominant here and thermal conductance increased from the S to PY anchor.

It is worth mentioning that thermal conductance is dominated by phonons in molecular junctions. For example, the room-temperature thermal conductance due to electrons and phonons in 4,4′-bipyridyl connected to gold electrodes are 0.17 pW/K and 34.8 pW/K, respectively [17]. This is because the off-resonance thermal conductance due to electrons is approximately proportional to electrical conductance from the Wiedemann–Franz law [12,32] (e.g., $\kappa_e = \alpha G$ where G is electrical conductance and $\alpha = 7.3 \times 10^{-6}$ at room temperature). Since molecules normally show a small electrical conductance, their thermal conductance due to electrons is small. Our result demonstrates that a suitable choice of anchor group can be used to suppress thermal conductance and enhance the thermoelectric figure of merit and efficiency of molecular thermoelectric devices.

3. Conclusions

In this paper, we investigated the effect of anchor groups on thermal conductance of single OPE3 molecules. We showed that thermal conductance is affected significantly by the choice of anchor group. The thermal conductance of OPE3 can be tuned between 20–35 pW/K at room temperature by choosing different anchor groups. Our calculations indicate that SMe is the better anchor to suppress thermal conductance for thermoelectricity, whereas pyridyl and carbodithioate are better choices for thermal management applications.

Author Contributions: Conceptualization, H.S.; calculations, M.D.N., S.S. and H.S. All authors have read and agreed to the published version of the manuscript.

Funding: This research was funded by the UKRI for Future Leaders Fellowship grant number MR/S015329/2 and the Leverhulme Trust for Early Career Fellowship grant number ECF-2018-375.

Institutional Review Board Statement: Not applicable.

Informed Consent Statement: Not applicable.

Data Availability Statement: The input files to reproduce simulation data can be found at: <https://warwick.ac.uk/nanolab>.

Conflicts of Interest: The authors declare no conflict of interest.

References

1. Disalvo, F.J. Thermoelectric cooling and power generation. *Science* **1999**, *285*, 703–706. [[CrossRef](#)]
2. Reddy, P.; Jang, S.Y.; Segalman, R.A.; Majumdar, A. Thermoelectricity in molecular junctions. *Science* **2007**, *315*, 1568–1571. [[CrossRef](#)] [[PubMed](#)]
3. Russ, B.; Glaudell, A.; Urban, J.J.; Chabiny, M.L.; Segalman, R.A. Organic thermoelectric materials for energy harvesting and temperature control. *Nat. Rev. Mater.* **2016**, *1*, 16050. [[CrossRef](#)]
4. Hasan, M.N.; Wahid, H.; Nayan, N.; Mohamed Ali, M.S. Inorganic thermoelectric materials: A review. *Int. J. Energy Res.* **2020**, *44*, 6170–6222. [[CrossRef](#)]
5. Evangeli, C.; Spiece, J.; Sangtarash, S.; Molina-Mendoza, A.J.; Mucientes, M.; Mueller, T.; Lambert, C.; Sadeghi, H.; Kolosov, O. Nanoscale Thermal Transport in 2D Nanostructures from Cryogenic to Room Temperature. *Adv. Electron. Mater.* **2019**, *5*, 1–10. [[CrossRef](#)]
6. Chen, H.; Sangtarash, S.; Li, G.; Gantenbein, M.; Cao, W.; Alqorashi, A.; Liu, J.; Zhang, C.; Zhang, Y.; Chen, L.; et al. Exploring the thermoelectric properties of oligo(phenylene-ethynylene) derivatives. *Nanoscale* **2020**, *12*, 15150–15156. [[CrossRef](#)] [[PubMed](#)]
7. Takaloo, A.V.; Sadeghi, H. Quantum Interference Enhanced Thermoelectricity in Ferrocene Based Molecular Junctions. *J. Nanosci. Nanotechnol.* **2019**, *19*, 7452–7455. [[CrossRef](#)] [[PubMed](#)]
8. Sangtarash, S.; Sadeghi, H.; Lambert, C.J. Connectivity-driven bi-thermoelectricity in heteroatom-substituted molecular junctions. *Phys. Chem. Chem. Phys.* **2018**, *20*, 9630–9637. [[CrossRef](#)]
9. Garner, M.H.; Li, H.; Chen, Y.; Su, T.A.; Shangguan, Z.; Paley, D.W.; Liu, T.; Ng, F.; Li, H.; Xiao, S.; et al. Comprehensive suppression of single-molecule conductance using destructive σ -interference. *Nature* **2018**, *558*, 415–419. [[CrossRef](#)]
10. Zotti, L.A.; Bürkle, M.; Pauly, F.; Lee, W.; Kim, K.; Jeong, W.; Asai, Y.; Reddy, P.; Cuevas, J.C. Heat dissipation and its relation to thermopower in single-molecule junctions. *New J. Phys.* **2014**, *16*, 015004. [[CrossRef](#)]
11. Lee, W.; Kim, K.; Jeong, W.; Zotti, L.A.; Pauly, F.; Cuevas, J.C.; Reddy, P. Heat dissipation in atomic-scale junctions. *Nature* **2013**, *498*, 209–212. [[CrossRef](#)] [[PubMed](#)]
12. Sadeghi, H. Theory of electron, phonon and spin transport in nanoscale quantum devices. *Nanotechnology* **2018**, *29*, 373001. [[CrossRef](#)] [[PubMed](#)]
13. Zhao, L.-D.; Lo, S.-H.; Zhang, Y.; Sun, H.; Tan, G.; Uher, C.; Wolverton, C.; Dravid, V.P.; Kanatzidis, M.G. Ultralow thermal conductivity and high thermoelectric figure of merit in SnSe crystals. *Nature* **2014**, *508*, 373–377. [[CrossRef](#)] [[PubMed](#)]
14. Liu, J.; van der Zee, B.; Alessandri, R.; Sami, S.; Dong, J.; Nugraha, M.I.; Barker, A.J.; Rousseva, S.; Qiu, L.; Qiu, X.; et al. N-type organic thermoelectrics: Demonstration of $ZT > 0.3$. *Nat. Commun.* **2020**, *11*, 5694. [[CrossRef](#)] [[PubMed](#)]
15. Al-Galiby, Q.H.; Sadeghi, H.; Algharagholy, L.A.; Grace, I.; Lambert, C. Tuning the thermoelectric properties of metallo-porphyrins. *Nanoscale* **2016**, *8*, 2428–2433. [[CrossRef](#)]
16. Sangtarash, S.; Sadeghi, H.; Lambert, C.J. Exploring quantum interference in heteroatom-substituted graphene-like molecules. *Nanoscale* **2016**, *8*, 13199–13205. [[CrossRef](#)]
17. Sadeghi, H. Quantum and Phonon Interference-Enhanced Molecular-Scale Thermoelectricity. *J. Phys. Chem. C* **2019**, *123*, 12556–12562. [[CrossRef](#)]
18. Sangtarash, S.; Sadeghi, H. Radical enhancement of molecular thermoelectric efficiency. *Nanoscale Adv.* **2020**, *2*, 1031–1035. [[CrossRef](#)]
19. Mosso, N.; Sadeghi, H.; Gemma, A.; Sangtarash, S.; Drechsler, U.; Lambert, C.; Gotsmann, B. Thermal Transport through Single-Molecule Junctions. *Nano Lett.* **2019**, *19*, 7614–7622. [[CrossRef](#)]
20. Cui, L.; Hur, S.; Akbar, Z.A.; Klöckner, J.C.; Jeong, W.; Pauly, F.; Jang, S.Y.; Reddy, P.; Meyhofer, E. Thermal conductance of single-molecule junctions. *Nature* **2019**, *572*, 628–633. [[CrossRef](#)]
21. Wang, K.; Meyhofer, E.; Reddy, P. Thermal and Thermoelectric Properties of Molecular Junctions. *Adv. Funct. Mater.* **2019**, *30*, 1904534. [[CrossRef](#)]
22. Rincón-García, L.; Evangeli, C.; Rubio-Bollinger, G.; Agrait, N. Thermopower measurements in molecular junctions. *Chem. Soc. Rev.* **2016**, *45*, 4285–4306. [[CrossRef](#)]
23. Klöckner, J.C.; Siebler, R.; Cuevas, J.C.; Pauly, F. Thermal conductance and thermoelectric figure of merit of C60-based single-molecule junctions: Electrons, phonons, and photons. *Phys. Rev. B* **2017**, *95*, 245404. [[CrossRef](#)]
24. Sadeghi, H.; Sangtarash, S.; Lambert, C.J. Oligoynes Molecular Junctions for Efficient Room Temperature Thermoelectric Power Generation. *Nano Lett.* **2015**, *15*, 7467–7472. [[CrossRef](#)] [[PubMed](#)]

25. Klöckner, J.C.; Cuevas, J.C.; Pauly, F. Tuning the thermal conductance of molecular junctions with interference effects. *Phys. Rev. B* **2017**, *96*, 1–10. [[CrossRef](#)]
26. Chen, R.; Sharony, I.; Nitzan, A. Local Atomic Heat Currents and Classical Interference in Single-Molecule Heat Conduction. *J. Phys. Chem. Lett.* **2020**, *11*, 4261–4268. [[CrossRef](#)]
27. Mosso, N.; Drechsler, U.; Menges, F.; Nirmalraj, P.; Karg, S.; Riel, H. Heat transport through atomic contacts. *Nat. Nanotechnol.* **2017**, *12*, 430–433. [[CrossRef](#)]
28. Sadeghi, H. Discriminating Seebeck sensing of molecules. *Phys. Chem. Chem. Phys.* **2019**, *21*, 2378–2381. [[CrossRef](#)]
29. Markussen, T. Phonon interference effects in molecular junctions. *J. Chem. Phys.* **2013**, *139*, 244101. [[CrossRef](#)]
30. Xiang, D.; Wang, X.; Jia, C.; Lee, T.; Guo, X. Molecular-Scale Electronics: From Concept to Function. *Chem. Rev.* **2016**, *116*, 4318–4440. [[CrossRef](#)]
31. Soler, J.M.; Artacho, E.; Gale, J.D.; García, A.; Junquera, J.; Ordejón, P.; Sánchez-Portal, D. The SIESTA method for ab initio order-N materials simulation. *J. Phys. Condens. Matter* **2002**, *14*, 2745–2779. [[CrossRef](#)]
32. Franz, R.; Wiedemann, G. Ueber die Wärme-Leitungsfähigkeit der Metalle. *Ann. Phys. Chem.* **1853**, *165*, 497–531. [[CrossRef](#)]